Analytical and Numerical Studies of a Steam Ejector on the Effect of Nozzle Exit Position and Suction Chamber Angle to Fluid Flow and System Performance

A. S. Ramesh and S. Joseph Sekhar[†]

Department of Mechanical Engineering, St. Xavier's Catholic College of Engineering, Nagercoil, Tamil Nadu, 629003, India

†*Corresponding Author Email: josephsekhar@hotmail.com*

ABSTRACT

Nozzle exit position [NXP] plays a vital role in the performance of the ejector, but its values are specified in a range for the required operating condition. In this study instead of the range of values, a specific value, named as entrainment diameter is developed and its effect on the performance of the ejector is studied for several combinations of suction chamber angle using numerical method. The effect of the condenser and boiler pressures on the performance of the ejector are also studied to ensure the off-design operating conditions. The entrainment diameter of an ejector is derived analytically by solving one dimensional compressible fluid flow equations using MATLAB. To study the effect of entrainment diameter on the performance of the ejector, CFD technique is employed. Analytical and numerical results are validated with experimental data available in the previous studies. For 7 kW refrigeration capacity, it is inferred that the suction chamber angle of 18° and the corresponding entrainment diameter 90.8 mm with the NXP of 23.62 mm yield the maximum entrainment ratio. The study predicts that the performance of the ejector is highly influenced by the pressure increment at the exit of the nozzle, while the suction chamber angle is between 12° to 21°.

Keywords: CFD; Entrainment diameter; Nozzle exit position; Steam jet ejector; Suction chamber angle.

NOMENCLATURE

A	area	**Subscripts**	
a	sound velocity	0,1,2,3,4,5	fluid states in respective cross section
C_p	specific heat at constant pressure		(Fig. 2)
D	diameter	a	active steam
E	total energy	cri	critical
Δh	change in enthalpy	e	primary nozzle exit
k	thermal conductivity	eff	effective
M	Mach number	en	entrainment
$\dot{m}$	mass flow rate	evap	evaporator
P	pressure, bar	exp	experiment
R	gas constant	i, j, k	space co-ordinates
T	temperature	m	mixing chamber
T	time	p	passive steam
u	velocity vector	t	primary nozzle throat
γ	specific heat ratio	**Superscript**	
δ_{ij}	Kronecker delta	*	primary flow choking condition
Θ	suction chamber and diffuser half angle, degree		
μ	dynamic viscosity	**Abbreviations**	
ρ	density	CFD	Computational Fluid Dynamics
τ_{ij}	shear stress tensor	COP	Co-efficient Of Performance
ω	ratio	ERS	Ejector Refrigeration System
		NXP	Nozzle Exit Position

1. INTRODUCTION

Most of the industries use heat as the driving energy for their required operations. Part of this low grade energy is utilized to get the desired output and the remaining part is rejected as waste heat. This waste energy can be effectively used for cogeneration purpose and to drive an Ejector Refrigeration System [ERS]. The simpler construction, robust design, low capital and maintenance costs and the use of eco-friendly refrigerants are the major advantages of this system (Eames *et al.* 2007; Cizungu *et al.* 2001; Ameur *et al.* 2015). Also, it can substantially reduce electricity consumption for refrigeration and air conditioning applications since the only element which consumes electric power in the cycle is a liquid refrigerant pump. The performance of this heat powered refrigeration cycle is lower than Vapour Absorption Refrigeration System [VARS] due to the complex compressible fluid flow in ejector. Though, due to its simpler construction and zero maintenance, ERS can fit better in heat powered refrigeration systems, and the careful design of the ejector can increase the performance of the system nearer to VARS. The co-efficient of the performance of ERS is directly proportional to the entrainment ratio of the ejector (Ruangtrakoon *et al.* 2011). The geometry and the operating conditions of the ejector influence the entrainment ratio (Varga *et al.* 2009). The effect of operating conditions on the performance of the ejector is relatively well established when compared with the geometrical effects (Ruangtrakoon *et al.* 2013; Varga *et al.* 2009; Sankarlal & Mani, 2005). The most influencing geometrical parameters over the performance of ejector are the area ratio (ratio of the area between constant area mixing chamber to primary nozzle throat), the primary nozzle exit position, the convergent angle of the constant pressure mixing section, and the length of constant area mixing section (Eames *et al.* 2007; Jia & Wenjian, 2012).

The effect of non-dimensional parameter (area ratio) on entrainment ratio is relatively well established when compared to the nozzle exit position. Moving the primary nozzle towards the mixing chamber decreases the entrainment ratio, but increases the critical back pressure (Eames *et al.* 2007; Pianthong *et al.* 2007; Aphornratana *et al.* 1997; Rusly *et al.* 2005; Chen *et al.* 2011). However, this prediction may not be true in all cases (Huang *et al.* 1999). In the previous studies, the initial value of NXP of the ejector, operating with any working fluid, was assumed to be based on the mixing chamber diameter. The ESDU design guide [7] predicts that the NXP value is 0.5 to 1.0 times the diameter of the mixing chamber. Yan *et al.* (2012), initially assumed the NXP value as 1.5 times the mixing chamber diameter and then varied it from 76% to 124%, to check its influence on the performance of the system. The same pattern was followed by Yan *et al.* (2016) for studying the effect of six geometrical parameters on the performance of the ejector. Aphornratana and Eames (1997) initially assumed the NXP as 0.5 to 1.0 times the mixing chamber diameter and then

studied various positions and concluded the optimum position as 0 to 0.833 times the mixing chamber's throat diameter. Varga *et al.* (2009) has assumed the value of NXP according to the ejector manufacturer's recommendation. Zhang *et al.* (2012) observed a good entrainment ratio while the value of NXP is 1.5 times of the mixing chamber diameter. Garcia del Valle *et al.* (2011) assumed the initial position of nozzle exit at anywhere within the suction chamber and analysed the effect of NXP on the performance of the ejector. Similar assumptions were made by Chen *et al.* (2015), to get the initial value of the NXP. All the investigations show a range of NXP for a specific operating condition. Therefore, developing an optimum NXP is the key need of the present research in ejector refrigeration system. Moving the primary nozzle towards the mixing chamber reduces the annular space between the active steam flying out from the nozzle and the wall of the suction chamber. And, this is the available area for the passive steam to start accelerating inside the ejector (Huang *et al.* 1999).

The available suction area for the passive steam to start accelerating has a major influence on the entrainment ratio (Ruangtrakoon *et al.* 2013). This available area can be same for different suction chamber angles with varying NXPs. Therefore, optimizing the entrainment diameter for a particular suction chamber angle simultaneously optimizes the NXP.

ASHRAE (ASHRAE, 1983) and ESDU (ESDU, 1985) have proposed the suction chamber and diffuser angles as 7-10° and 3-4° respectively, however this range is not suitable for all the fluids and operating conditions as well (Zhu *et al.* 2009). Therefore, it is clear that the geometrical parameters, especially the annular area available for the passive steam to start accelerating has the major role in the performance. Moreover the effect of entrainment diameter and the suction chamber angle have to be studied further to enhance the performance of the ejector.

In this work, an analytical model of the ejector has been generated in MATLab for deriving the various geometrical factors like primary nozzle throat and exit diameters, mixing chamber diameter, entrainment diameter and the corresponding NXP based on the compressible fluid flow equations. This study mainly focuses on the effect of area available for the passive steam to get accelerated inside the ejector and to predict the specific NXP for a particular operating condition. As the suction chamber angle is proportional to NXP and the existing analytical models do not predict the suction chamber angle, numerical modelling has been used in this study to analyse the various combinations of suction chamber angle and the entrainment diameter. The analytical and the numerical results are validated by the experimental values reported in the literature. The boiler pressure, and condenser pressure are varied for a fixed evaporator temperature to check the impact of the variations in operating parameters on the entrainment ratio.

2. SYSTEM DESCRIPTION

A schematic view of the ejector refrigeration system is shown in Fig. 1. It consists of a boiler, ejector, evaporator, condenser, expansion valve and liquid pump. The various stages in the system is marked as 1 to 6. High pressure steam generated from low grade energy [1] is allowed to expand through the convergent-divergent nozzle of the ejector to obtain supersonic velocity. This expanded steam possesses high momentum and the part of this momentum is lost to entrain the saturated steam from the evaporator at a low pressure [2]. Thus makes the rest of fluid in evaporator to get cooled. Both of these fluids get mixed in the mixing chamber of the ejector and their pressure is partially recovered from a set of shock waves. Further pressure increment is achieved by a diffuser [3]. The steam leaving the ejector is condensed in a condenser [4] and part of the condensed liquid goes to evaporator as makeup liquid through an expansion device [5], and the remaining part is pumped to the boiler [6]. The performance of the ejector refrigeration system is given by,

$$(COP)_{ERS} = \frac{\Delta h_{evaporator}}{\Delta h_{generator}} \times \frac{\dot{m}_p}{\dot{m}_a} = \frac{\Delta h_{evaporator}}{\Delta h_{generator}} \times \omega$$

(1)

Therefore it is obvious that the COP of the system is completely dependent on the entrainment ratio.
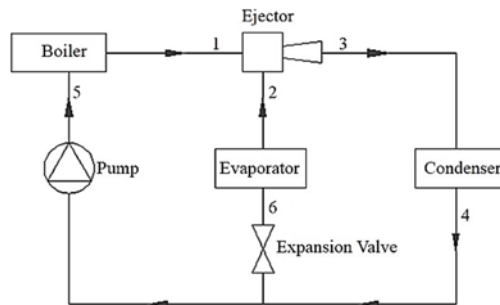

Fig. 1. Schematic view of an ejector refrigeration system.

3. ANALYTICAL AND NUMERICAL SIMULATION

The flow chart of combined analytical and numerical simulation is shown in Fig. 2. The key dimensions of the ejector such as nozzle throat and exit, entrainment and the mixing chamber diameters are derived from one dimensional compressible fluid flow equations. As the suction chamber angle cannot be derived analytically, the derived diameters are given as input to the numerical simulation where the suction chamber angle is assumed based on ASHRAE and ESDU standards. Further the combination of suction chamber angle and the entrainment diameter are modelled and analysed in a CFD software.

The condition of the ejector is chosen to operate it with low grade energy sources. Also, it should be compatible with working steam. Therefore, for the analytical study, the boiler pressure is chosen as 2 bar

which means the system can work with the heat from a heat source of temperature close to 150 °C. And the application of this system can be an air-conditioning system. Therefore, the evaporator temperature is chosen as 10° C. For this condition, a 7 kW (2 TR refrigeration) ejector is designed analytically and analyzed numerically. The operating parameters are given in Table 1.
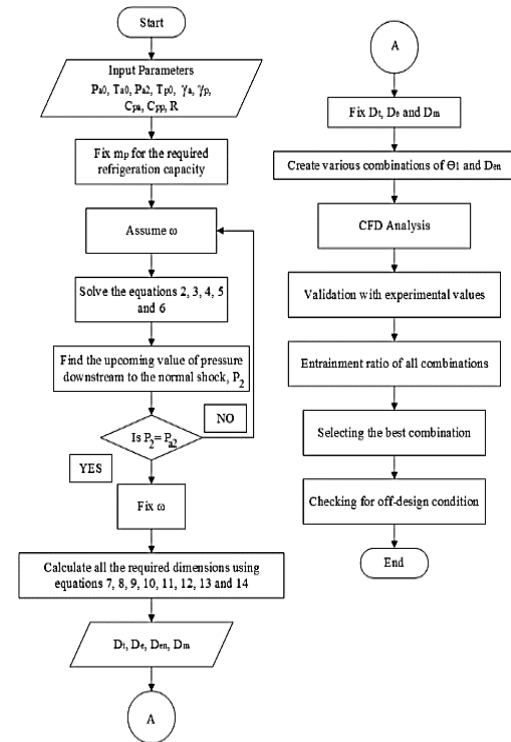

Fig. 2. Flow chart for the analytical and numerical simulation.

Table 1 Operating condition of the ejector

Operating parameters	Values
Refrigeration capacity, W	7000
Boiler pressure, bar	2
Boiler temperature, K	393.2
Evaporator pressure, bar	0.0122
Evaporator temperature, K	283
Suction pressure, bar	0.006
Condenser pressure, bar	0.045
Condenser temperature, K	304

3.1 Analytical Simulation

The schematic diagram given in Fig. 3 shows the various components and their arrangements in an ejector. Sections 0 to 5 are taken along the ejector for the convenient description of the flow.

For the simplification of analytical model the following assumptions, such as one dimensional flow, steady state, adiabatic walls, isentropic flow in section from 0 to 5 except a frictional loss of 5% (Bartosiewicz *et al.* 2005) in the divergent portion

of primary nozzle and negligible kinetic energy at the inlet of primary nozzle, suction port and exit of diffuser (Huang *et al.* 1999), both the primary and secondary fluids are chocked, secondary fluid is chocked at section 3 of the ejector, the primary fluid is dry saturated, complete mixing of the primary and secondary fluid within the mixing chamber and constant-pressure mixing of primary and secondary fluids are considered. A normal shock is usually developed in between the sections 3 and 4 (Bartosiewicz *et al.* 2005), therefore, in addition to the assumptions made, a normal shock at section 4 is assumed. The required thermo-physical properties of the fluid are taken from the property database REFPROP (NIST Standard Reference Database 23, 1980). All the equations are derived from the basic compressible fluid flow equations (Cengal and Cimbala, 2010). Based on the required refrigeration capacity mass flow rate of the passive steam is fixed. Any value less than one is initially assumed as entrainment ratio. From the adiabatic energy equation along the primary nozzle the Mach number at the exit of nozzle is obtained and it is as:

$$M_{a2}^* = 0.95 * \sqrt{\left(\frac{\gamma_a+1}{\gamma_a-1}\right)\left(1 - \left(\frac{P_{ao}}{P_{a2}}\right)^{\frac{\gamma_a-1}{\gamma_a}}\right)} \quad (2)$$
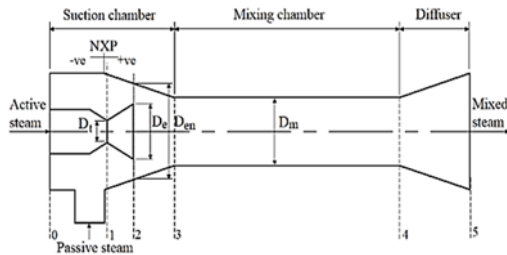

Fig. 3. Schematic diagram of an ejector.

The obtained Mach number shows that the active steam flow is supersonic and it possesses high momentum. The part of the momentum in the active steam is spent to entrain the passive steam from the evaporator. Therefore the impulse function after mixing will be equal to the difference between the impulse function of active and passive steam. Solving for impulse function, the Mach number at section 3 is derived and it is given as:

$$M_3^* = M_{a2}^* * \frac{\left(\frac{1}{1+\omega}\right) + \left(\frac{\omega}{\omega+1}\right)\left(\frac{a_p^*}{a_a^*}\right)\left(\frac{M_{p2}^*}{M_{a2}^*}\right)}{\sqrt{\left(\frac{1}{1+\omega}\right) + \left(\frac{\omega}{\omega+1}\right)\left(\frac{a_p^*}{a_a^*}\right)^2}} \quad (3)$$

Where, $\left(\frac{a_p^*}{a_a^*}\right)$ is the local sound velocity ratio between passive and active steam and it is given by:

$$\left(\frac{a_p^*}{a_a^*}\right) = \sqrt{\frac{C_{pp} \times T_{po} \times \left(\frac{2 \times C_{pa}}{R_a} - 1\right)}{C_{pa} \times T_{ao} \times \left(\frac{2 \times C_{pp}}{R_p} - 1\right)}} \quad (4)$$

Due to the supersonic flow and the difference of pressure, a normal shock is formed and as mentioned before, it is assumed to be formed in section 4. Pressure ratio across the shock is the ratio between

the condenser pressure and pressure before shock. That is, the ratio between the pressure in section 5 to pressure just before section 4. By the basics of compressible fluid flow, the pressure ratio across the normal shock in section 4 is given by:

$$\left(\frac{P_5}{P_2}\right) = \left(\frac{\left[\frac{\gamma_3+1}{\gamma_3-1}\right]M_3^*-1}{\left[\frac{\gamma_3+1}{\gamma_3-1}\right]M_3^{*2}}\right)\left(1 + \left(\left(\frac{M_3^{*2}}{M_3^{*2}-\left[\frac{\gamma_3-1}{\gamma_3+1}\right]}\right)^{\frac{\gamma_3}{\gamma_3-1}} 1\right)\right) \quad (5)$$

Specific heat ratio at the mixing chamber γ_3 is calculated by weighted average and it is given as:

$$\gamma_3 = \left(\frac{1}{1+\omega}\right)\gamma_a + \left(\frac{\omega}{1+\omega}\right)\gamma_p \quad (6)$$

The pressure before the shock has to be equal to the required evaporator pressure. If the upcoming downstream pressure of the shock wave is not equal to the required evaporator pressure, the assumed entrainment ratio will be altered. When the downstream pressure is less than the required evaporator pressure, the entrainment ratio will be increased. If it is not the case, the entrainment ratio is decreased. By this procedure the actual entrainment ratio is calculated. Depending on this ratio, by applying momentum equation in sections 1, 2, and 3, various areas at the throat, exit of primary nozzle, annular entrainment for passive steam at section 2, and mixing chamber are calculated from equations 7, 8, 9 and 13.

The chocking mass flow rate in the primary nozzle ($\dot{m}_a$) is given by,

$$\frac{\dot{m}_a}{A_t \times P_{ao}} \times \sqrt{\frac{T_{ao} \times R_a}{\gamma_a}} = \left(\frac{2}{\gamma_a+1}\right)^{\frac{\gamma_a+1}{2(\gamma_a-1)}} \quad (7)$$

From the above equation, area of nozzle throat can be calculated for the chocking condition.

Again by applying continuity equation in section 2, exit area of the primary nozzle can be found as given below,

$$\left(\frac{A_e}{A_t}\right) = \left(\frac{1}{M_{a2}^{*2}}\right) \times \left[\left(\frac{2}{\gamma_a+1}\right) + \left(\frac{\gamma_a-1}{\gamma_a+1} \times M_{a2}^{*2}\right)\right]^{\left(\frac{\gamma_a+1}{2 \times (\gamma_a-1)}\right)} \quad (8)$$

The positioning of the ejector nozzle inside the suction chamber is decided based on the suction area or entrainment area, and it can be calculated as given below:

$$A_{en} = \frac{m_p}{P_2} \times \sqrt{R_p \times Tp_o} \times \left[\frac{1 - \left(\frac{\gamma_p-1}{\gamma_p+1} \times M_{p2}^{*2}\right)}{M_{p2}^* \times \sqrt{\frac{2 \times \gamma_p}{\gamma_p+1}}}\right] \quad (9)$$

The mixing chamber diameter is determined by considering the total mass flow rate of both the primary and secondary fluids, temperature, pressure and critical Mach number of the section.

The temperature (T_m), gas constant (R_m) and the ratio of specific heat (γ_m) of mixed stream are obtained from the equations 10, 11 and 12.

$$T_m = \frac{(m_a \times T_{ao}) + (m_p \times T_{po})}{m_a + m_p} \quad (10)$$

$$R_m = \frac{(m_a \times R_{ao}) + (m_p \times R_{po})}{m_a + m_p} \tag{11}$$

$$\gamma_m = \frac{\gamma_a}{1+\omega} + \frac{\omega \times \gamma_p}{1+\omega} \tag{12}$$

The continuity equation is solved for finding the constant area mixing chamber and it is given by:

$$A_m = \frac{(m_a + m_p) \times \sqrt{R_m \times T_m}}{P_2} \times \left[\frac{1 - \left(\frac{\gamma_m - 1}{\gamma_m + 1} \times M_3^{*2} \right)}{M_3^* \times \sqrt{\frac{2 \times \gamma_m}{\gamma_m + 1}}} \right] \tag{13}$$

3.2 Numerical Simulation

The complex flow in ejector has led to increasing reliance on CFD as a design tool (Fan *et al*. 2011) and many researchers have agreed with CFD for predicting results closer to the experimental values (Rusly *et al*. 2005; Ruangtrakoon *et al*. 2013; Sriveerakul *et al*. 2007).

The entrainment diameter of 87.8 mm is analytically derived and few diameters above and below this value as given in Table 2 are taken for further numerical analysis. The convergent angles have been taken from 4 to 22^0. The other dimensions from the analytical simulation are held constant and they are shown in Table 2.

Table 2 Dimensions of numerically simulated ejector

Geometrical Parameters	Input values for numerical simulation
Suction chamber angle, deg	4 to 22
Entrainment diameter, mm	80.8 :1: 93.8
Nozzle throat diameter, mm	7.2
Nozzle exit diameter, mm	33.4
Mixing chamber diameter, mm	60.9
Diffuser divergence angle, deg	8

The CFD code selected for the simulation is the FLUENT module in ANSYS 13. The model is created in 2D domain and 3D effects have been modelled by using the axisymmetric solver. As the flow expected is supersonic, turbulence compressible flow has to be modelled. The governing equations for compressible fluid (ANSYS FLUENT User's Guide, 2010) in the compact Cartesian form are:

$$\frac{\partial \rho}{\partial t} + \frac{\partial}{\partial x_i} (\rho u_i) = 0 \tag{14}$$

$$\frac{\partial}{\partial t} (\rho u_i) + \frac{\partial}{\partial x_j} (\rho u_i u_j) = -\frac{\partial P}{\partial x_i} + \frac{\partial \tau_{ij}}{\partial x_j} \tag{15}$$

$$\frac{\partial}{\partial t} (\rho E) + \frac{\partial}{\partial x_i} (u_i(\rho E + \rho)) = \nabla.\left(\alpha_{eff} \frac{\partial T}{\partial x_i} \right) + \nabla.\left(u_j(\tau_{ij}) \right) \tag{16}$$

$$\tau_{ij} = \mu_{eff} \left(\frac{\partial u_i}{\partial x_j} + \frac{\partial u_j}{\partial x_i} \right) - \frac{2}{3} \mu_{eff} \frac{\partial u_k}{\partial x_k} \delta_{ij} \tag{17}$$

Pressure-based solver has been selected to solve the governing equations. As the active steam flying out of the primary nozzle is modelled to have supersonic

velocity, the Reynolds number is around 7×10^6 and hence the flow is turbulent. But the secondary fluid flow from the evaporator has very low Reynolds number of around 2000. Therefore, it is necessary to select a turbulent model which can accurately predict both the high and lower Reynolds number flow. The turbulence model k-ε-RNG is such a model which can accurately handle both the higher and lower Reynolds number (ANSYS FLUENT User's Guide, 2010). Also, in the previous studies this model was chosen and were used effectively (Chen *et al*. 2011; Zhu *et al*. 2009; Bartosiewicz *et al*. 2005). This model relies on the Boussinesq hypothesis. According to this hypothesis, the momentum transfer caused by molecular motion in gases which can be described by a molecular viscosity Reynolds stress tensor is proportional to the traceless deformation rate tensor.

$$\rho u_i u_j = \mu_t \left(\frac{\partial u_i}{\partial x_j} + \frac{\partial u_j}{\partial x_i} \right) - \frac{2}{3} \left(\rho k + \mu_t \frac{\partial u_i}{\partial x_i} \right) \delta_{ij} \tag{18}$$

The main advantage of this approach is the relatively low computational cost associated with the determination of the turbulent viscosity (Bartosiewicz, Aidoun, Desevaux, and Mercadier, 2005). The boundary conditions are selected as pressure inlet and pressure outlet. Steam is assumed as an ideal gas because, for the lower operating conditions, as used here, the variation of results between the real gas model and the ideal gas model is quite negligible (Sriveerakul *et al*. 2007).

3.3 Validation with the Available Experimental data

The results from the analytical and numerical simulation were validated with the experimental data available in literature (Ruangtrakoon *et al*. 2011) for an ejector with the dimensions given in Table 3.

Table 3 Dimensions of the ejector used for validation

Geometrical parameters, mm	Dimensions of experimental ejector
Nozzle inlet diameter	7.5
Nozzle throat diameter	2.6
Nozzle exit diameter	11.63
Nozzle exit position	23
Mixing chamber diameter	19
Mixing chamber length	114
Suction chamber length	130
Subsonic diffuser length	180
Ejector outlet diameter	40

Analytical and numerical simulation methods have been used to calculate the entrainment ratio for this ejector for the given boiler, evaporator and condenser temperatures of 111.2 °C, 7.5 °C and 32.33 °C respectively.

Table 4 Experimental and simulated results

Ejector	T_{boiler} (°C)	T_{evap} (°C)	ω	Error, ω (%)
Experiment	111.2	7.5	0.262	-
Analytical Simulation	111.2	7.5	0.342	30.65
Numerical Simulation	111.2	7.5	0.31	18.32

Table 4 gives the comparison between theoretical results and the experimental values reported in the literature. The analytical values of entrainment ratio are higher than the values in literature. This deviation is mainly due to the assumptions made in analytical simulation. While comparing the numerical simulation results, the entrainment ratio is also higher than the experimental values. The possible reason for this deviation might be due to some assumptions like perfect gas, frictionless and adiabatic walls and so on. Therefore the deviation of this simulated result from the experimentation is tolerable. And, therefore, the same procedure is used for further numerical analysis with the dimensions derived.

4. RESULTS AND DISCUSSION

It is known that entrainment ratio is the factor which decides the performance of the ejector. Therefore, for various combinations of entrainment diameter and suction chamber angles the entrainment ratio is derived. The obtained results are investigated with the help of post-processing facility in CFD software. Contours of Mach are predominantly used to analyse the flow within the ejector.

4.1 Flow Within Ejector

The contour of Mach number along the ejector for the suction chamber angle of 18° and the entrainment diameter of 90.8 mm is shown in Fig. 4. At the exit of the convergent divergent nozzle there forms the first series of oblique shock. In case of over expanded wave these shock waves are not so strong wherein under expanded wave it gives a strong barrier to the flow. It is clear from the figure that for all the models, the expanding wave from the primary nozzle is over-expanded as the flying wave from the nozzle is having a convergence angle. This type of wave is more desirable for the ejector's performance (Ruangtrakoon *et al*. 2011). The flying primary fluid from the nozzle exit and the suction chamber wall forms a convergent duct. This causes the secondary fluid from the evaporator to get accelerated and to choke at some position of that convergent duct. The annular area corresponding to this is known as effective area (Huang *et al*. 1999). Therefore, for the optimum performance, the ejector must be operated at double-choking mode. The gradual mixing of active and passive steam happens after passing through the effective area. During the mixing, the momentum of the primary fluid is gradually transferred to the secondary fluid. After mixing, due to high pressure in downstream, a series of secondary oblique shock waves are created. Due to these shock waves and diffuser, the mixed fluid obtains its required condensing pressure.
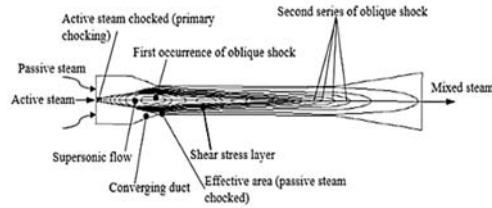

Fig. 4. Mach contour for $\Theta_1 = 18°$ and $D_{en} = 90.8$ mm.

4.2 Effect of Suction Chamber Angle and Entrainment Diameter

The influence of entrainment diameter on the entrainment ratio for various suction chamber angles is shown in Fig. 5. Each entrainment diameter has its own corresponding NXP depending on the suction chamber angle.
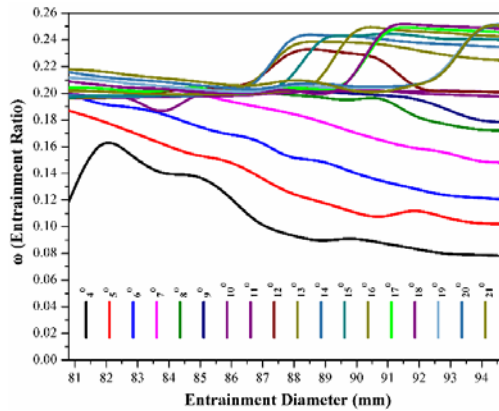

Fig. 5. Effect of various suction chamber angles over entrainment ratio for a range of entrainment diameter.
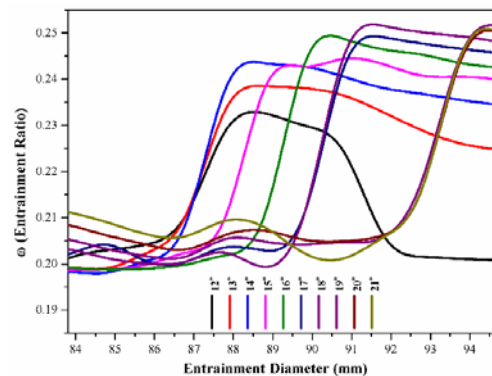

Fig. 6. Variation of entrainment ratio of the suction chamber angles of 12° to 21°.

Fig. 5 shows that the entrainment ratio decreases with increase in entrainment diameter upto the suction chamber angle of 7°. This shows that, upto 7° moving the primary nozzle away from the mixing chamber reduces the entrainment ratio. For the
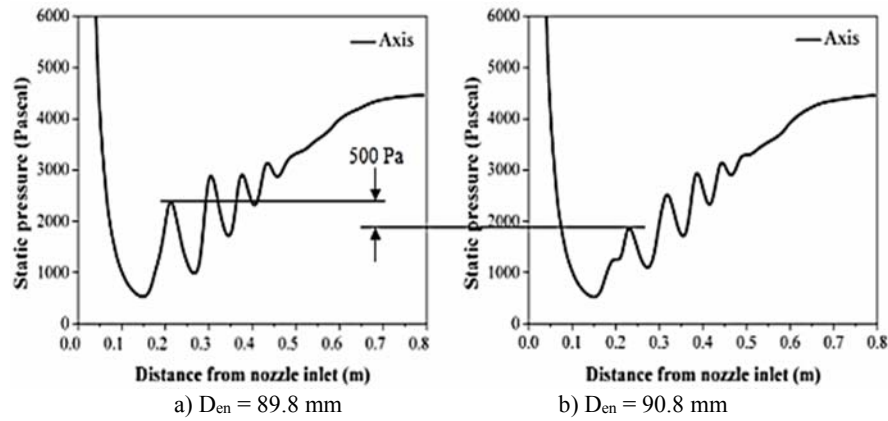
a) D_{en} = 89.8 mm   b) D_{en} = 90.8 mm

Fig. 7. Variation of static pressure along the axial distance of ejector from nozzle inlet for the suction chamber angle of 18°.

suction chamber angles of 8°, 9°, 10°, 11° and 12°, the entrainment ratio increases with increase in entrainment diameter upto the entrainment diameters of 86.8 mm, 87.8 mm, 90.8 mm, 88.8 mm and 87.8 mm respectively and then started to decrease. This shows that, from 8° to 12° moving the primary nozzle away from the mixing chamber increases the entrainment ratio upto the entrainment diameters mentioned, after which it gets reduced. At the suction chamber angle of 12^0, a steep increment of entrainment ratio at some entrainment diameter has been observed.

As shown in Fig. 6, after this particular entrainment diameter, entrainment ratio decreases gradually. This phenomenon existed up to 21° after which the increment and decrement of the entrainment ratio are found to be gradual and there is no significant increment.

The reason behind this flow phenomenon can be explained by Fig. 7. Fig. 7 (a) shows that the increase in static pressure at the exit of primary nozzle is higher when compared to the static pressure increase in the subsequent entrainment diameter as shown in Fig. 7 (b). The difference in pressure between each entrainment diameters is found to be 500 Pa. The entrainment diameter, which gives the maximum entrainment ratio and all the entrainment diameters above that have lower increase in static pressure at the exit of primary nozzle. This trend has been found to be similar for all the suction chamber angles from 12 to 21°.

The entrainment diameters having maximum entrainment ratio and their subsequent ones for the suction chamber angles of 12 to 21° are presented in Table 5. The corresponding entrainment ratio, nozzle exit position and the difference in static pressure are also presented. After 21°, for the entire entrainment diameters, there was no such steep increment in entrainment ratio. The reason for the increase in pressure at the exit of the nozzle is due to the formation of the first series of oblique shock waves. If these shock waves are strong, it will provide a strong barrier to the primary fluid flow from the nozzle. Therefore, the pressure increases and consequently, the momentum of the primary fluid

reduces and by which the flow cannot be smooth. This decrement in momentum will reduce the entrainment of secondary fluid; subsequently the entrainment ratio decreases. In all the cases, the second shock position is identical and it shows that the ejector can be operated at higher critical condenser pressure. Also, the maximum entrainment ratio is obtained while the nozzle is moved away from the mixing chamber, which in turn increases the annular area available for the passive steam to get accelerated.

Table 5 Difference in pressure increment at the nozzle exit zone for various suction chamber

Θ_1, deg	D_{en}, mm	NXP, mm	ω	ΔP, Pa
12	86.8	45.52	0.2066	315
	87.8	43.16	0.2333	
13	86.8	41.91	0.2055	370
	87.8	39.74	0.2392	
14	86.8	38.80	0.2018	458
	87.8	36.80	0.2457	
15	87.8	34.24	0.2032	459
	88.8	33.38	0.2461	
16	88.8	30.25	0.2026	542
	89.8	28.51	0.2520	
17	89.8	26.74	0.2032	542
	90.8	25.10	0.2506	
18	89.8	25.16	0.2038	500
	90.8	23.62	0.2535	
19	92.8	19.39	0.2136	500
	93.8	17.93	0.2525	
20	92.8	18.34	0.2106	583
	93.8	16.97	0.2520	
21	92.8	17.39	0.2100	490
	93.8	16.09	0.2533	

4.3 Effect of Condenser Pressure

The performance curve shown in Fig. 8 explains the effect of condenser pressure (back pressure for ejector) on the entrainment ratio. The performance curve is divided into three categories: choked flow (both active and passive streams were choked), unchoked flow (active steam is alone choked), and reversed flow (both fluids are not chocked and the active steam is forced into the evaporator). To get the maximum entrainment ratio the ejector must be operated at choked flow region and this region is separated from the unchoked flow region by critical pressure.
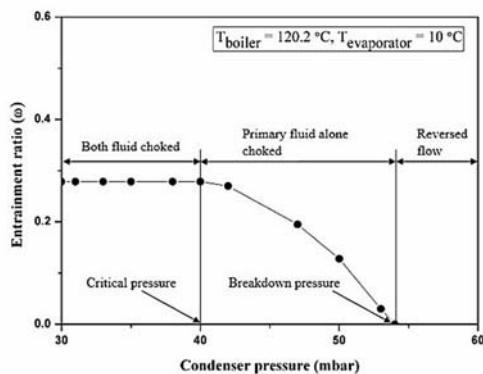

Fig. 8. Effect of back pressure (condenser pressure) over entrainment ratio for $\Theta_1 = 18°$ and $D_{en} = 90.8$ mm.

The reason behind this can be explained with the help of Mach contours for various condenser pressure and it is shown in Fig. 9.
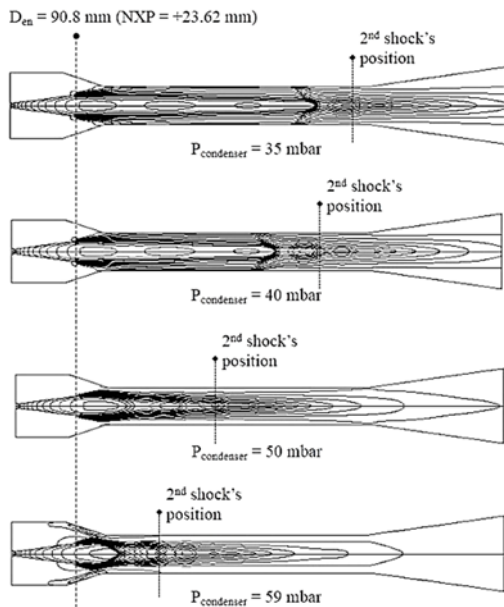

Fig. 9. Effect of back pressure (condenser pressure) on the contour of Mach number.

With the increase in condenser pressure the second series of oblique shock gets stronger. As the condenser pressure increases the shock wave moves towards the mixing chamber. Due to this, the mixing phenomenon of passive steam with the primary steam gets disturbed, and with the further increase in condenser pressure the shock wave gets very strong and the entrainment of passive steam is prevented. For the operating condition defined in this study, the breakdown pressure is found to be 59 mbar. From 59 mbar to 40 mbar ejector can operate with the single choking condition, that is, active steam alone gets choked and the passive steam is not given with enough space to get choked in the mixing chamber. Below 40 mbar, ejector was able to operate with double-choking mode, which is more desirable for the higher performance of the ejector. This is due to the fact that in this mode, passive steam is allowed to get choked. As the mass flow rate of passive steam reaches its maximum limit, the entrainment ratio will be maximized. The pressure corresponding to this performance is known as critical pressure, which also varies with the change in other operating and geometrical conditions.

4.4 Effect of the Boiler Pressure

The effect of boiler pressure on entrainment ratio for various condenser pressure is given in Fig. 10. It can be clearly seen that, with the increase in boiler pressure, the critical back pressure is increased. This shows that ejector can be operated at higher condensing temperature with double chocking mode. But on the other hand, with the increase in boiler pressure, the entrainment ratio is decreased.
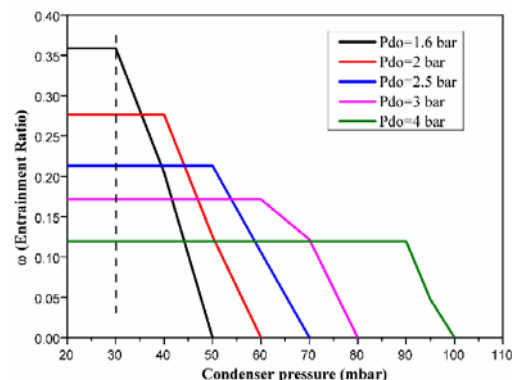

Fig. 10. Effect of boiler pressure on entrainment ratio for various condenser pressure.

The physical phenomenon behind this trend can be explained with the help of Mach contours in Fig. 11. All the Mach contours in Figure 11 reveal that both the active and passive steams are chocked. The second shock wave position moves towards the exit of the ejector as the boiler pressure is increased. This means, for the same condenser pressure of 30 mbar, the second shock wave has a different location for an increase in boiler pressure. As it is moving towards the exit, the ejector can be operated at higher critical pressure. But on the other hand the annular area between the expanding wave from the nozzle and the suction chamber wall decreases as the pressure is increased. This is due to the higher momentum of the primary fluid. Therefore the area available for suction steam to mix with primary fluid decreases and as a result the entrainment ratio is decreased.
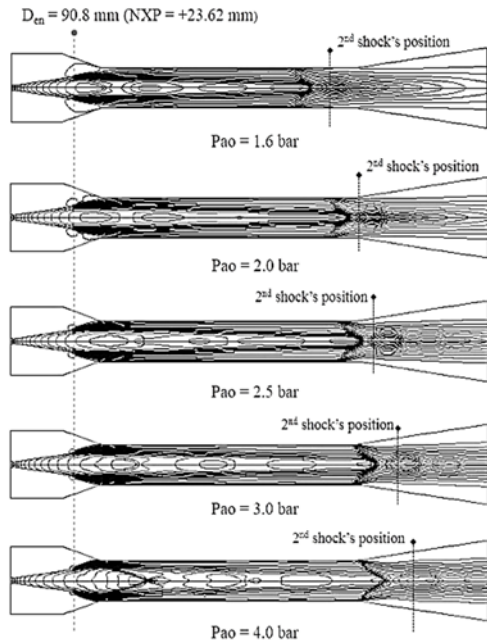
Fig. 11. Effect of active steam pressure on the contour of Mach number.

5. CONCLUSION

In this study, an analytical simulation using MATLAB was carried out to derive the various important diameters of the ejector and then, a numerical simulation using ANSYS Fluent software was employed to investigate the effect of entrainment diameter for various suction chamber angles over the performance of the ejector. Based on the studies, the following conclusions are made:

- The variation in results between numerical simulation and the literature experimental data available in the literature was found to be 18.32%. This proves that CFD is an effective tool for predicting the flow characteristics within the steam ejector.

- Upto the suction chamber angle of 7°, entrainment ratio decreases with the increase in entrainment diameter. This also means that entrainment ratio decreases with the decrease in NXP. For suction chamber angle between 8 and 11°, entrainment ratio increases upto certain increment in entrainment diameter, and then starts to decrease.

- From and above 12° suction chamber angle, at some entrainment diameters, there is a sudden increment in entrainment ratio, which has been found to be maximum, and above that particular entrainment diameter, the change in entrainment ratio is gradual. This phenomenon existed upto 21° and after which there is no such steep increment. Primary shock waves emerging at the primary nozzle exit zone are found to be responsible for the sudden increment in entrainment ratio.

- The maximum entrainment ratio was obtained at the suction chamber angle of 18° with the entrainment diameter 90.8 mm. The corresponding NXP is 23.62 mm. For this suction chamber angle, at the boiler pressure of 2 bar, the critical back pressure was inferred as 40 mbar and the breakdown pressure was 59 mbar.

- With the increase in back pressure, the critical back pressure increases along with the decrease in entrainment ratio. The second series shock wave produced in the mixing chamber has a significant impact on entrainment ratio and the critical back pressure.

For all the suction chamber angle there is a specific NXP value which yields a maximum entrainment ratio and it will change with the variations in operating conditions only.

REFERENCES

Ameur, K., Z. Aidoun and M. Ouzzane (2015). Analysis of the critical conditions and the effect of slip in two-phase ejectors. *Journal of Applied Fluid Mechanics* 9, Special Issue 2, 213-222.

ANSYS FLUENT User's Guide (2010). ANSYS, Inc. Southpointe, Canonsburg, PA.

Aphornratana, S. and I. W. Eames (1997). A small capacity steam-ejector refrigerator: experimental investigation of a system using ejector with movable primary nozzle. *International Journal of Refrigeration* 20, 352-355.

Ashrae. (1983). *Steam Jet Refrigeration Equipment.* In: Equipment Handbook, Atlanta, GA, USA: ASHRAE, Chapter 13.

Bartosiewicz, Y., Z. Aidoun, P. Desevaux and Y. Mercadier (2005). Numerical and experimental investigations on supersonic ejectors. *International Journal of Heat and Fluid Flow* 26, 56-70.

Cengal, Y. A. and J. M. Cimbala (2010). *Fluid Mechanics Fundamentals and Applications*, 3rd Ed., McGraw-Hill, New York.

Chen, S., G. C. Chen and L. Fang (2015). An experimental study and 1-D analysis of an ejector with a movable primary nozzle that operates with R236fa. *International Journal of Refrigeration* 60, 19-25.

Chen, W., D. Chong, J. Yan and J. Liu (2011). Numerical optimization on the geometrical factors of natural gas ejectors. *International Journal of Thermal Sciences* 50, 1554-1561.

Cizungu, K., A. Mani and M. Groll (2001). Performance comparison of vapour jet refrigeration system with environment friendly working fluids. *Applied Thermal Engineering* 21, 585-598.

Eames, I. W., A. E. Ablwaifa and V. Petrenko (2007). Results of an experimental study of an advanced jet-pump refrigerator operating with R245fa. *Applied Thermal Engineering* 27, 2833-2840.

ESDU (1985). Ejector and jet pump, data item 86030. *ESDU International Ltd, London, UK.*

Fan, J., J. Eves, H. M. Thompson, V. V. Toropov, N. Kapur, D. Copley and A. Mincher (2011). Computational fluid dynamic analysis and design optimization of jet pumps. *Computers and Fluids* 46, 212-217.

Garcia del Valle, J., J. Saiz Jabardo, F. C. Ruiz, J. San Jose Alonso (2011). A one dimensional model for the determination of an ejector entrainment ratio. *International Journal of Refrigeration* 35, 772-784.

Huang, B. J., J. M. Chang, C. P. Wang and V. A. Petrenko (1999). A 1-D analysis of ejector performance. *International Journal of Refrigeration* 22, 354-364.

Jia, Y. and C. Wenjian (2012). Area ratio effects to the performance of air-cooled ejector refrigeration cycle with R134a refrigerant. *Energy Conversion and Management* 53, 240-246.

NIST Standard Reference Database 23 (1980). NIST Thermodynamics and Transport Properties of Refrigerants and Refrigerant Mixtures. REFPROP, Version 9.1.

Pianthong, K., W. Seehanam, M. Behnia, T. Sriveerakul and S. Aphornratana (2007). Investigation and improvement of ejector refrigeration system using computational fluid dynamics technique. *Energy Conversion and Management* 48, 2556-2564.

Ruangtrakoon, N., S. Aphornratana and T. Sriveerakul (2011). Experimental studies of a steam jet refrigeration cycle: Effect of the primary nozzle geometries to system performance. *Experimental Thermal and Fluid Science* 35, 676-683.

Ruangtrakoon, N., T. Thongtip, S. Aphornratana and T. Sriveerakul (2013). CFD simulation on the effect of primary nozzle geometries for a steam ejector in refrigeration cycle. *International Journal of Thermal Sciences* 63, 133-145.

Rusly, E., L. Aye, W. W. S. Charters and A. Ooi (2005). CFD analysis of ejector in a combined ejector cooling system. *International Journal of Refrigeration* 28, 1092-1101.

Sankarlal, T. and A. Mani (2005). Experimental studies on an ammonia ejector refrigeration system. *International Communications in Heat and Mass Transfer* 33, 224-230.

Sriveerakul, T., S. Aphornratana and K. Chunnanond (2007). Performance prediction of steam ejector using computational fluid dynamics, Part 1. Validation of the CFD results. *International Journal of Thermal Sciences* 46, 812-822.

Varga, S., A. C. Oliveiraa and B. Diaconu (2009). Influence of geometrical factors on steam ejector performance a numerical assessment. *International Journal of Refrigeration* 32, 1694-1701.

Yan, J., W. Cai and Y. Li (2012). Geometry parameters effect for air-cooled ejector cooling systems with R134a refrigerant. *Renewable Energy* 46, 155-163.

Yan, J., C. Lin, W. Cai, H. Chen and H. Wang (2016). Experimental study on key geometric parameters of an R134A ejector cooling system. *International Journal of Refrigeration*.

Zhang, B., X. Song, J. Lv and J. Zuo (2012). Study on the key ejector structures of the waste heat-driven ejector air conditioning system with R236fa as working fluid. *Energy and Buildings* 49, 209-215.

Zhu, Y., W. Cai, C. Wen and Y. Li (2009). Numerical investigation of geometry parameters for design of high performance ejectors. *Applied Thermal Engineering* 29, 898-905.